Available online at www.sciencedirect.com
SCIENCE DIRECT
Colloids and Surfaces A: Physicochem. Eng. Aspects 267 (2005) 103–109
COLLOIDS AND SURFACES A
www.elsevier.com/locate/colsurfa

Atomistic simulation of KCl transport in charged silicon nanochannels: Interfacial effects

R. Qiao, N.R. Aluru*

Department of Mechanical and Industrial Engineering, Beckman Institute for Advanced Science and Technology, University of Illinois at Urbana-Champaign, Urbana, IL 61801, USA

Available online 16 August 2005

Abstract

Electroosmotic flow is an important fluid transport mechanism in nanofluidic systems. In this paper, we investigate the ion distribution and velocity profiles of KCl solution in two oppositely charged silicon nanochannels by using molecular dynamics simulations. The continuum theories, based on the Poisson–Boltzmann equation and the Navier–Stokes equations, predict that the distribution of the counter-ions, water flux and ionic conductivity in the two oppositely charged channels are the same. However, molecular dynamics simulations show very different results. First, the counter-ion distributions are substantially different in the two channels. Second, the water flux and ionic conductivity in the two channels differ by a factor of more than three. Third, the co-ion fluxes are in the opposite direction. The different counter-ion distributions in the two channels are attributed to the different size of the K^+ and Cl^- ions and the discreteness of the water molecules, and the asymmetric dependence of the water and ion transport is attributed to the asymmetric dependence of the hydrogen bonding of water near the charged silicon surface, which influences the dynamic behavior of interfacial water significantly.

Keywords: Electroosmotic flow; Nanofluidics; Hydrogen bonding; Electrical double layer; Molecular dynamics

1. Introduction

Electroosmotic flow is widely encountered in many biological and engineering systems [1,2]. The basic concept of electroosmotic flow can be summarized as follows: when an ionic solution is in contact with a charged surface, an electrical double layer (EDL) with a net positive or negative charge develops near the surface. If an external electrical field is applied in the direction tangential to the surface, the fluid will be dragged by the moving ions in the EDL and an electroosmotic transport is generated. The most important observables in electroosmotic flow are the ion distribution and the velocity profile in the channel. Because of its scalability and ease-of-control, electroosmotic transport is widely used in many microfluidic systems, and its application in nanofluidic systems is gaining increasing attention in the recent years [3–6]. For example, Bohn and co-workers studied the effect of surface charge and ionic strength on the electroosmotic transport through nuclear-track-etched nanopore membrane [5], in which the pore diameter is on the order of 10–100 nm. More recently, nanopores as narrow as one nanometer have been fabricated by using focused ion beam drilling, and electrokinetic transport in these nanopores has been studied experimentally [7,8].

Modeling and simulation of electroosmotic flow in nanometer wide channels can address many of the fundamental issues currently facing the design of nanofluidic systems [6]. At present, the simulation of electroosmotic flow is primarily based on the classical continuum theories, i.e., the Poisson–Boltzmann equation for the ion distribution and Navier–Stokes equations for the fluid transport [9–11]. In the Poisson–Boltzmann equation, the ions are modeled as point charges and the water is modeled as a dielectric

* Corresponding author at: Department of Mechanical & Industrial Engineering, University of Illinois at Urbana-Champaign, 3265 Beckman Institute, 405 N. Mathews mc 251, Urbana, IL 61801, USA.
E-mail address: aluru@uiuc.edu (N. Aluru).
URL: http://www.uiuc.edu/ aluru.

0927-7757/$ – see front matter © 2005 Elsevier B.V. All rights reserved.
doi:10.1016/j.colsurfa.2005.06.067

continuum. Therefore, the molecular nature of the ion and the discreteness of the water molecules are not accounted for in the Poisson–Boltzmann equation. Likewise, in the Navier–Stokes equations, water is modeled as a continuum medium with a constant viscosity, and the effect of the surface–water interactions is accounted for as a velocity boundary condition. Therefore, the physics at the atomistic length scales, such as density oscillations near the surface, and the effect of confinement are not accounted for. Though these atomistic details may be neglected in microscale channels, they can become dominant in nanofluidic systems, where the surface-to-volume ratio is very high and the critical dimension is comparable to the size of the fluid molecules.

Atomistic simulation, and in particular Molecular Dynamics (MD) simulation, is an important tool to study fluid flow in nanometer wide channels. In an MD simulation, ion–ion, ion–wall and ion–water interactions are calculated explicitly, the trajectory of the system is integrated by using classical mechanics and various measurables, e.g., ion concentration and bulk velocity, are obtained from statistical averaging. By using proper interaction potentials between the atoms in the system, an MD simulation can provide a quantitative understanding of the various physical processes involved without relying on the many assumptions built into the continuum theory. However, MD simulations are usually computationally very expensive, and compared to the continuum simulations, they are relatively less widely employed at present. The few studies on electroosmotic flow in nanochannels using MD indicated that to describe the ion distributions accurately, one needs to account for the molecular nature of the water/ions in detail, and to model the velocity profile accurately, one needs to account for the fluid–surface interactions on the transport properties of interfacial fluids [12–18]. Though the finite size effect of ions has been accounted for in many theoretical studies on the ion distribution in the electrical double layer [19–23], the influence of the molecular nature of water on the ion distribution is beginning to draw a significant attention only recently [24,25]. Similarly, even though the effect of surface–fluid interactions on the transport properties of fluid has already been realized [1,2], a molecular level understanding of the mechanism is currently missing.

In this paper, we present a study of the electroosmotic transport and ionic conductivity of a KCl solution in two silicon nanochannels with opposite surface charge densities. Specifically, we investigated how the ion distribution is influenced by the finite size of the ion and the water molecules, and how the electroosmotic transport is influenced by the surface–fluid interactions. The rest of the paper is organized as follows: in Section 2 we present the MD simulation details; in Section 3, we discuss ion distributions in nanochannels; and in Section 4, we discuss how the dynamic properties of interfacial water, and thus the electroosmotic flow, are influenced by the surface charge. Finally, Section 5 presents the conclusions.

2. Simulation methods

Fig. 1 shows the schematic diagram of the channel system. The system consists of a slab of KCl solution (or water) sandwiched between two channel walls. Each wall is made up of four layers of silicon atoms oriented in the ⟨1 1 1⟩ direction. The lateral dimensions of the channel wall are 4.66 nm × 4.22 nm. The channel width, defined as the distance between the two innermost wall layers, is 3.49 nm. The silicon atoms in the innermost layer of the channel wall (layer I of the lower channel wall and its counterpart in the upper channel wall, see Fig. 1) were assigned small partial charges to produce the desired surface charge density, σ_s. Water is modeled by using the SPC/E model [26] and ions are modeled as charged Lennard–Jones (LJ) atoms. The LJ parameters for the O–O and Si–O pairs were taken from the Gromacs force field [27], and the LJ parameters for the ion–ion and ion–O pairs were taken from [28].

Non-equilibrium MD simulations were performed with a modified Gromacs 3.0.5 [27]. Instead of using a non-equilibrium MD simulation, electroosmotic flow can also be investigated by using the linear response theory and equilibrium MD simulations [17]. Periodic boundary conditions are used in the x- and y-directions. The temperature of the fluid was maintained at 300 K by coupling the fluid atoms to a Nose thermostat [29]. To avoid biasing the velocity profile, only the velocity component in the direction orthogonal to the flow was thermostated [30]. The electrostatic interactions are computed by using the PME algorithm with a slab correction [31], and all other interactions are computed by using a cut-off scheme with a cut-off radius of 1.1 nm. Other simulation details can be found in [14]. Starting from a random configuration, the system was simulated for 1.0 ns to reach steady-state. After that, a production run of 5–15 ns was performed. The electroosmotic flow was driven by an external electrical field, E_{ext}, applied along the channel in the x-direction. Because of the extremely high thermal noise, a strong electrical field ($|E_{ext}| = 0.25$ V/nm) was used in our simulations so that the fluid velocity can be retrieved with reasonable accuracy. Table 1 summarizes the simulations performed in this paper.

3. Ion distribution in nanochannels

Fig. 2 shows the concentration profiles of Cl^- ion and water across the channel for case 1, where the surface charge density is 0.13 C/m^2. The co-ion (K^+ ion) concentration is not shown as its magnitude is small and thus its contribution to the electroosmotic flow is also small. The Cl^- ion concentration obtained from the Poisson–Boltzmann (PB) equation (see [14] for details on the PB equation and its numerical solution) is also shown for comparison. In solving the PB equation, the dielectric constant of water is taken as 80, and the position of the wall is taken to coincide with the first concentration peak of the Cl^- ion obtained from the MD simulation. We observe that (1) the first concentration peak

of the counter-ion (Cl^- ion) is about 81% higher compared to the PB prediction, and (2) the counter-ion concentration does not decrease monotonically to its value in the channel center as PB equation predicts. These observations are similar to those reported in [13,14]. As discussed in [14], the first observation is mainly caused by the attractive non-electrostatic interactions between the Cl^- ion and the channel wall atoms, and the second observation is mainly caused by the interactions between the ion and its hydration water molecules, and is strongly correlated to the oscillation of the water concentration near the surface.

Fig. 3 shows the concentration profiles of K^+ ion and water across the channel for case 2, where the surface charge density is $-0.13\,C/m^2$. Since the PB equation does not account for the different size of K^+ and Cl^- ions, the K^+ ion concentration in case 2 obtained from the PB equation is identical to that of the Cl^- ion concentration in case 1 ($\sigma_s = 0.13\,C/m^2$). However, MD simulation indicated that the K^+ ion concentration in case 2 is substantially different from that of the Cl^- ion concentration in case 1. Specifically, the K^+ ion concentration profile shows two distinct peaks, which are located at 0.27 and 0.50 nm away from the channel surface. Such a difference is mainly caused by the different size of the K^+ and Cl^- ions (the bare diameter of a K^+ and a Cl^- ion are 0.27 and 0.36 nm, respectively [32]) and the discreteness of the water molecules.

In an electrolyte solution, the water molecules near an ion are loosely bonded to the ion due to the strong charge–dipole interactions between the ion and the water molecules. These water molecules are usually referred to as the hydration water of the ion. As the charge–dipole interactions between an ion and its hydration water are highly attractive, losing part or all of its hydration water is an energetically unfavorable process for an ion. The accumulation of counter-ions very close to the channel wall ($z \approx 0.27$ nm) is primarily due to the ion–ion and ion–surface interactions. The second peak observed at $z \approx 0.50$ nm is due to the accumulation of counter-ions to maximize the number of their hydration water molecules. To understand this quantitatively, we computed the hydration number of K^+ ion across the channel in case 2. The hydration number of an ion is defined as the number of water molecules within the first hydration shell of an ion, and the radius of the first hydration shell (r_{min}) is usually defined as the location of the first minimum of the ion–water radial distribution function (RDF) [33]. The radius of the hydration shell of a K^+ ion is found to be 0.37 nm (see Fig. 4(c)). Fig. 4(a) and (b) show the correlation between the concentration distribution and hydration number of the K^+ ion in case 2. We observe that the second K^+ ion concentration peak corresponds very well with the maximum of the K^+ ion hydration number in the channel. This confirms that the second concentration peak of the K^+ ion concentration is mainly caused by the interactions between the K^+ ion and its hydration water molecules. Since the charge–dipole interactions between an ion and its hydration water molecules are weaker for larger ions, the hydration effect is less important for the larger ions. For example, a similar analysis for Cl^- ion distribution in case 1 indicated that the hydration number of the Cl^- ion reaches a maximum at a position of 0.60 nm away from the channel surface, and this give rise to a very weak peak in the Cl^- concentration profile at a position of 0.62 nm away from the channel surface.

4. Electroosmotic flow in nanochannels

4.1. Water and ion transport

Fig. 5 compares the water velocity profiles for cases 1 and 2 as obtained from continuum and MD simulations. In the continuum simulation, we used the ion distribution obtained from the MD simulation as input to the Stokes equation:

$$\frac{\mathrm{d}}{\mathrm{d}z}\left(\mu\frac{\mathrm{d}u_{eo}(z)}{\mathrm{d}z}\right) + \sum_{i=1}^{N} e\tilde{z}_i c_i(z) E_{ext} = 0 \tag{1}$$

where $u_{eo}(z)$ and $c_i(z)$ are the electroosmotic velocity and ion concentration across the channel, respectively, μ is the dynamic viscosity of the fluid, N is the number of ion species in the channel (here $N = 2$), e is the electron charge (i.e., 1.6×10^{-19} C), and $\tilde{z}_i$ is the valency of ion i. The continuum theory predicts a similar velocity in both cases (the prediction would be identical if the ion concentrations are obtained by solving the Poisson–Boltzmann equation), while the MD results predict that u_{eo} in a negatively charged channel is much higher compared to that in a positively charged channel, and the difference in u_{eo} between the two cases is mainly due to the different velocity behavior in the region of about 5 Åfrom the channel wall.

In addition to the water transport, we also studied the ionic transport. In the present simulations, the flux J_i for an ionic specie i has two components, namely, an electrical migration component

$$J_i^{mig} = \int_0^W \mu_i^e(z)\tilde{z}_i c_i(z) E_{ext}\,\mathrm{d}z \tag{2}$$

and a convection component

$$J_i^{eo} = \int_0^W u_{eo}(z) c_i(z)\,\mathrm{d}z \tag{3}$$

where $\mu_i^e(z)$ is the electrophoretic mobility of ion i at position z, W is the channel width. The conductivity of the electrolyte in the channel is given by

$$\kappa = \sum_{i=1}^{N} \frac{\tilde{z}_i e J_i}{W E_{ext}} \tag{4}$$

Table 2 shows the ionic fluxes and their various components in cases 1 and 2. The ionic fluxes are dramatically different in the two cases. Specifically, (a) the counter-ion flux density in case 2 is 4.38 times of that in case 1, and (b) the co-ion fluxes are in the opposite direction. Observation

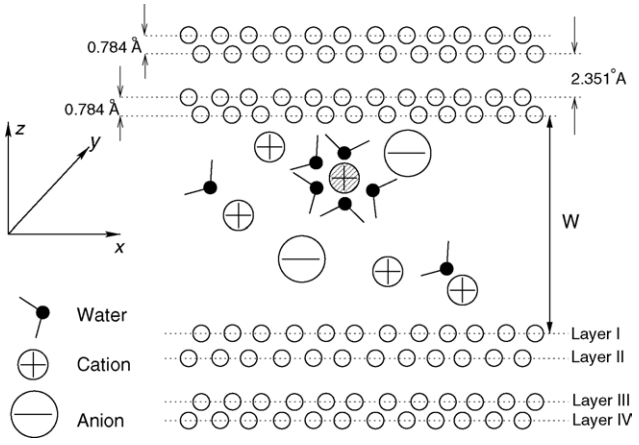

Fig. 1. A schematic diagram of the channel system under investigation. The two channel walls are symmetrical with respect to the channel center line. The channel width W is defined as the distance between the two innermost wall layers. For the coordinate system chosen, $z = 0$ corresponds to the central plane of the channel system.

(a) can be understood by noting that both the convection and the electrical migration components of the counter-ion flux are stronger in case 2 than in case 1. Observation (b) can be understood by noting that though the electrical migration components of the co-ion fluxes are comparable in both cases, the convection component of the co-ion flux in case 2 is much stronger than that of case 1. The strong convection component dominates the overall co-ion transport in case 2, and this leads to the opposite overall transport of the co-ions. Table 2 also shows that the ionic conductivity in case 2 is 3.77 times of that of case 1, even though the number of ions and magnitude of the surface charge are identical in both cases.

Phenomenologically, the above results can be attributed to the different dynamic behavior of the water and ions near the charged surfaces, i.e., the water viscosity μ is much higher (and the counter-ion mobility $\mu_i^e(z)$ is lower) near a positively charged surface compared to that near a negatively charged surface. The dependence of the water viscosity and the ion mobility on the surface charge has been reported, and was mainly attributed to the layering effect of water, the strong electrical field near the surface and the high local ion concentration [2,1]. However, the asymmetric effect of surface charge, to our knowledge, is not known, and it is difficult to explain such an asymmetric effect by the aforementioned mechanisms. This is because, in both cases, the water concentration near the surface is very similar and $|\sigma_s|$ is identical. We have also performed simulations using other electrolytes, e.g., NaF, for which the ion distributions in the two oppositely charged channels are only slightly different, but similar asymmetric effects were observed. Therefore, the asymmetric effects are not caused by the different ion distribution near the channel surface. We will show that such asymmetric effects originate mainly from the different hydrogen bonding of the interfacial water in the two cases.

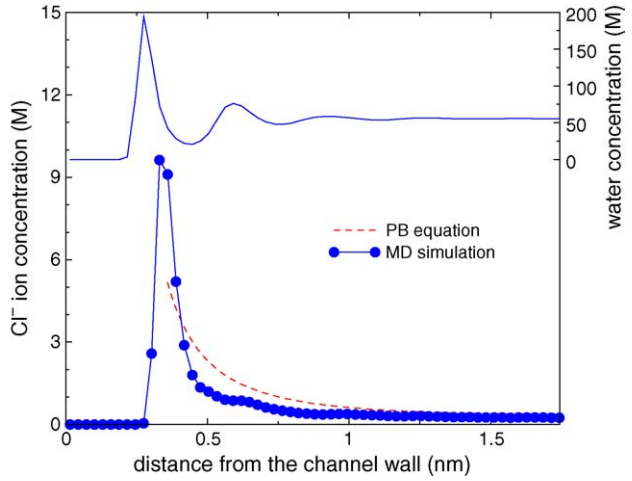

Fig. 2. Cl^- ion and water concentration profiles across the channel in case 1 ($\sigma_s = 0.13\,C/m^2$).

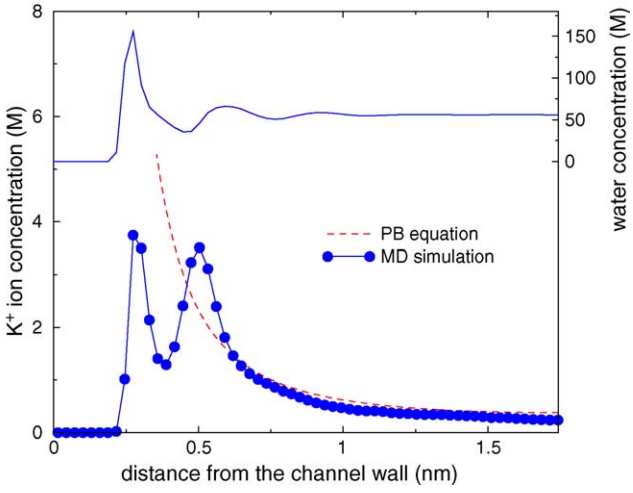

Fig. 3. K^+ ion and water concentration profiles across the channel in case 2 ($\sigma_s = -0.13\,C/m^2$).

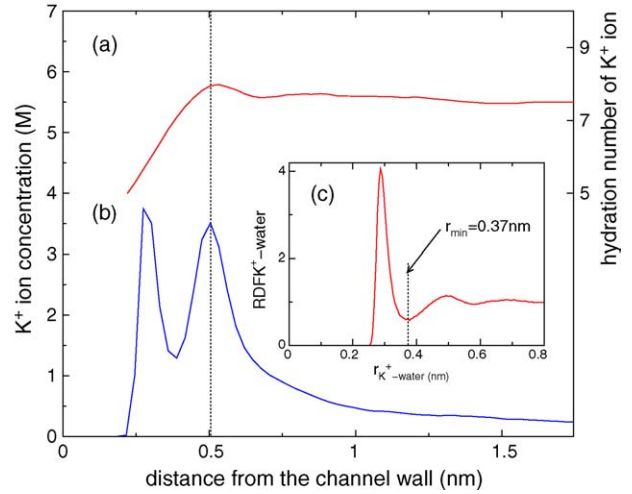

Fig. 4. (a) Variation of the hydration number for the K^+ ion across the channel in case 2 ($\sigma_s = -0.13\,C/m^2$). (b) K^+ ion concentration across the channel for case 2. (c) Radial distribution function of K^+-water in the bulk.

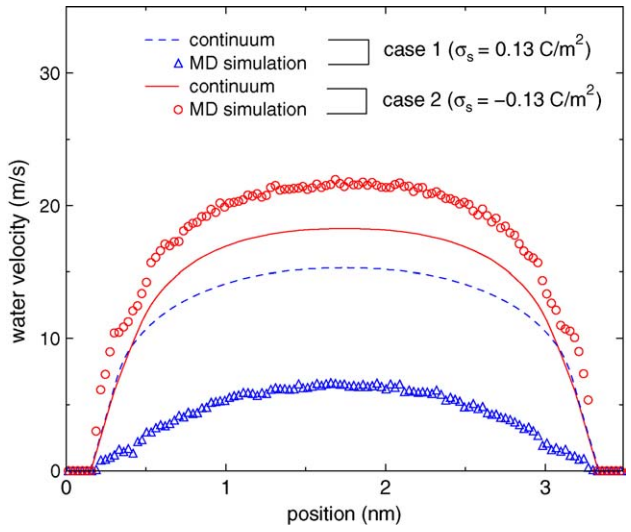

Fig. 5. Comparison of the velocity profile for cases 1 and 2, as obtained from the continuum theory and MD simulations. In the continuum simulation, a no-slip boundary condition is applied at a position of 0.16 nm from the surface – this is consistent with the MD observation. A constant viscosity of $\mu = 0.736$ mPa s is used.

4.2. Hydrogen bonding of the interfacial water

Hydrogen bonding (HB) plays a crucial role in determining the various properties of water, e.g., viscosity, surface tension, and temperature dependence of density. Because of its importance in determining the properties of the interfacial water, the hydrogen bonding of interfacial water has been studied extensively in the past [34–39]. These studies have greatly improved our understanding of the structure and dynamics of the interfacial water. However, there are relatively few studies on how the hydrogen bonding is influenced by the surface charge, which is ubiquitous in nanofluidic systems.

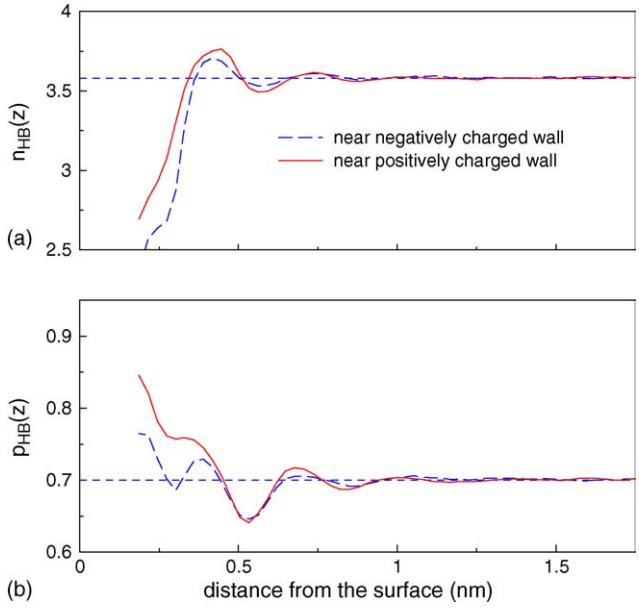

Fig. 6. (a) The variation of the average number of hydrogen bonds [$n_{HB}(z)$] that a water molecule participates in, as a function of the water–surface distance. (b) Bonding percentage $p_{HB}(z)$ as a function of water–surface distance.

To study the influence of surface charge on the hydrogen bonding of interfacial water, we performed equilibrium MD simulation for case 3, where the lower and upper wall have a charge density of +0.13 C/m^2 and −0.13 C/m^2, respectively. The system contains 2114 water molecules and no ions. There is no applied external electrical field. We adopted the geometric definition of hydrogen bonding used in [40], namely, two water molecules are considered to be hydrogen-bonded if (a) the O–O distance is less than 3.5 Å, and (b) the O–H···O angle (hydrogen bond angle θ_{HB}), is less than 30°. To characterize the hydrogen bonding of the water molecules, we introduce a bonding percentage $p_{HB} = n_{HB}/n_{r=0.35}$ [39], where n_{HB} is the number of water molecules that are hydrogen-bonded to a given water molecule, and $n_{r=0.35}$ is the total number of water molecules that are within 0.35 nm from the given water molecule. A high p_{HB} corresponds to a state that water molecules are highly bond-ordered, and the water behaves more "ice-like".

Fig. 6(a) and (b) show the variation of the average number of hydrogen bonds [$n_{HB}(z)$] that a water molecule participates in and the bonding percentage [$p_{HB}(z)$] as a function of the distance between the water molecule and the positively and negatively charged surfaces. We observe that, near both surfaces, though $n_{HB}(z)$ decreases as we approach the channel surface ($z < 0.40$ nm), the bonding percentage $p_{HB}(z)$ increases at the same time. We also observe that both $n_{HB}(z)$ and $p_{HB}(z)$ are notably higher near the positively charged surface than near a negatively charged surface. This indicates that the water near a positively charged surface shows a higher degree of hydrogen bonding compared to that near a negatively charged surface, i.e., the surface charge has an asymmetric effect on the hydrogen bonding of interfacial water. A molecular level understanding of such a phenomena can be obtained by analyzing the orientation of the O–H bond of the interfacial water molecules and considering the directional preference for hydrogen bonding between water molecules.

Fig. 7(a) shows the density profile of the oxygen atoms near the charged surface, and Fig. 7(b) and (c) show the orientation distribution of the O–H bond of the water molecules near the positively and the negatively charged surface, respectively. When the surface is positively charged, the O–H bonds of the water molecules at point 1 are oriented mainly at 50–95° with respect to the surface, indicating that the O–H bonds of the water molecule point mainly away or parallel to the surface. As the water moves away from the surface, one of its O–H bonds tends to point towards the surface and its second O–H bond tends to point away from the surface. Such an orientation pattern helps to maximize the number of hydrogen bonds. For example, a water molecule at point 1 can serve as hydrogen bond donor and acceptor for the water molecules above it (e.g., water at points 2 and 3) at the same time. Because a large amount of O–H bonds of the water at points 2 and 3 orient at 90–110°, it is not difficult for water

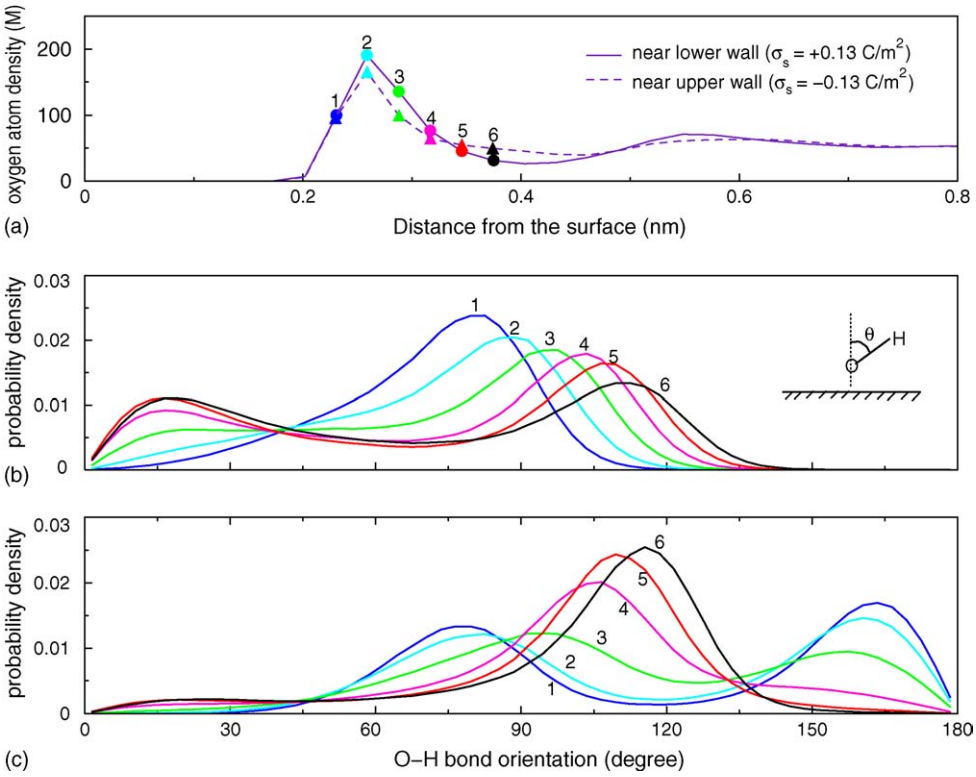

Fig. 7. (a) Oxygen atom density profile of the water molecules near the positively and the negatively charged wall in case 3. (b) and (c) Probability distribution for the O—H bond orientation of water near the positively charged wall and the negatively charged wall, respectively. The curves in panels (b) and (c) correspond to the different locations of the oxygen atom as shown in panel (a), e.g., curve 1 of panel (b) shows the O—H bond orientation of the water molecules whose oxygen atom is located at point 1 in panel (a).

Table 1
Summary of the simulations performed

Case no.	Lower/upper wall charge density (C/m^2)	Molecules in system water/K^+/Cl^-	E_{ext} (V/nm)	Simulation time (ns)
1	0.13/0.13	2094/3/35	−0.25	16
2	−0.13/ − 0.13	2124/35/3	0.25	16
3	0.13/-0.13	2114/0/0	0	6

molecules at point 1 (acceptor) and points 2 and 3 (donor) to form hydrogen bonds.

However, the situation is quite different near the negatively charged surface. Fig. 7(c) indicates that for water molecules at point 1, one of their O–H bonds points towards the surface, and the second O–H bond orients at 60–90°. As the water molecules move away from the surface, such a bimodal distribution becomes weaker and at point 6, most of the O–H bonds orient at 100–130°. Compared to that near a positively charged surface, such an orientation pattern is less favorable for maximizing the number of hydrogen bonds. For example, water molecules at point 1 can form at most three hydrogen bonds with its neighbors as one of its O–H bonds points towards the surface. In addition, for a water molecule at point 3, its O–H bond orientation has a large component at $\theta > 110°$. Though it can still serve as donor for the hydrogen bond with

Table 2
Ionic flux density and conductivity in electroosmotic flows [a]

Case 1 ($\sigma_s = 0.13$ C/m^2)	Case 2 ($\sigma_s = -0.13$ C/m^2)
Counter-ion flux (kmol/m^2 s)	
$J^{eo}_{Cl^-} = 2.264$	$J^{eo}_{K^+} = 12.915$
$J^{mig}_{Cl^-} = 3.612$	$J^{mig}_{K^+} = 12.805$
$J_{Cl^-} = 5.876$	$J_{K^+} = 25.720$
Co-ion flux (kmol/m^2 s)	
$J^{eo}_{K^+} = 0.412$	$J^{eo}_{Cl^-} = 1.503$
$J^{mig}_{K^+} = -1.210$	$J^{mig}_{Cl^-} = -0.969$
$J_{K^+} = -0.798$	$J_{Cl^-} = 0.534$
Conductivity (S/m)	
$\kappa_1 = 2.571$	$\kappa_2 = 9.704$

[a] A flux is denoted positive if it is in the positive x-direction, and negative otherwise.

water at points 1 and 2, such a hydrogen bond will break easily. This is because for a water at point 3 to form an optimal hydrogen bond (i.e., a hydrogen bond with a hydrogen bond angle $\theta_{HB} = 0$) with water at points 1 and 2, its O–H bond orientation angle cannot exceed 102° (the z-direction spacing between points 1 and 3 is 0.6 Å; assuming a hydrogen bond length of 3.0 Å, we have the O–H bond orientation with respect to the horizontal line to be $\sin^{-1}(0.6/3) \approx 12°$). From this discussion, it is clear that the different hydrogen bonding characteristics for water near two oppositely charged surfaces is mainly caused by the different orientation of water near the charged surfaces. The dynamic properties of water depend strongly on the hydrogen bonding of the water molecules. For example, compared to liquids with similar molecular weight, water has a very large viscosity (at 293 K, the dynamic viscosity of water is 1.0 mPa s, while that of *n*-pentane is only 0.24 mPa s though the latter has a molecular weight four times that of water [41]). A stronger hydrogen bonding between the water molecules retards the passage of water molecules around each other, and thus leads to a higher viscosity. Therefore, the asymmetric dependence of the hydrogen bonding of interfacial water on the surface charge will lead to the asymmetric dependence of the viscosity of the interfacial water on the surface charge, which further leads to the asymmetric dependence of the electroosmotic transport on the surface charge.

5. Conclusions

In this paper, we have presented a molecular dynamics study of the electroosmotic transport and ionic conductivity of a KCl solution in two silicon nanochannels with opposite surface charge densities. Though the classical continuum theories predict that the ion distribution and the water/ion transport are the same in both channels, MD simulations show a very different picture. The counter-ion distributions are substantially different near the channel wall, and the water flux and ionic conductivity in the two channels differ by a factor of more than 3. The different ion distributions in the two cases is primarily due to the different size of the K^+ and Cl^- ions and the discreteness of the water molecules. The difference in water/ion transport originates mainly from the asymmetric dependence of the hydrogen bonding of the interfacial water. Specifically, for the same magnitude of surface charge density, the water molecules near a positively charged surface show a higher degree of hydrogen bonding compared to that near a negatively charged surface. This then leads to a higher viscosity of the interfacial water near the positive surface, which further leads to a weaker electroosmotic flow in the positively charged channel.

Acknowledgement

This research was supported by the waterCAMPWS at the University of Illinois at Urbana-Champaign.

References

[1] R. Hunter, Zeta Potential in Colloid Science: Principles and Applications, Academic Press, London, UK, 1981.
[2] J. Lyklema, Fundamentals of Interface and Colloid Science, Academic Press, San Diego, CA, 1995.
[3] C.H. Lin, R.J. Yang, C.H. Tai, C.Y. Lee, L.M. Fu, J. Micromech. Microeng. 14 (2004) 639.
[4] L.Q. Ren, D. Sinton, D.Q. Li, J. Micromech. Microeng. 13 (2003) 739.
[5] P.J. Kemery, J.K. Steehler, P.W. Bohn, Langmuir 14 (1998) 2884.
[6] T.C. Kuo, L.A. Sloan, J.V. Sweedler, P.W. Bohn, Langmuir 17 (2001) 6298.
[7] J. Li, D. Stein, C. Mcmullan, D. Branton, M.J. Aziz, J.A. Golovchenko, Nature 412 (2001) 166.
[8] A. Meller, L. Nivon, D. Branton, Phys. Rev. Lett. 86 (2001) 3435.
[9] S.V. Ermakov, S.C. Jacobson, J.M. Ramsey, Anal. Chem. 70 (1998) 4494.
[10] M.J. Mitchell, R. Qiao, N.R. Aluru, J. MEMS 9 (2000) 435.
[11] H. Daiguji, P.D. Yang, A. Majumdar, Nano Lett. 4 (2004) 137.
[12] J. Lyklema, S. Rovillard, J.D. Coninck, Langmuir 14 (1998) 5659.
[13] J. Freund, J. Chem. Phys. 116 (2002) 2194.
[14] R. Qiao, N.R. Aluru, J. Chem. Phys. 118 (2003) 4692.
[15] R. Qiao, N.R. Aluru, Nano Lett. 3 (2003) 1013.
[16] R. Qiao, N.R. Aluru, Phys. Rev. Lett. 92 (2004) 198301.
[17] V. Marry, J.F. Dufreche, M. Jardat, P. Turq, Mol. Phys. 101 (2003) 3111.
[18] A.P. Thompson, J. Chem. Phys. 119 (2003) 7503.
[19] R. Andreu, M. Molero, J.J. Calvente, C.W. Outhwaite, L.B. Bhuiyan, Electrochim. Acta 41 (1996) 2125.
[20] S. Lamperski, C.W. Outhwaite, J. Electroanal. Chem. 460 (1999) 135.
[21] H. Greberg, R. Kjellander, J. Chem. Phys. 108 (1998) 2940.
[22] R. Kjellander, H. Greberg, J. Electroanal. Chem. 450 (1998) 233.
[23] I. Borukhov, D. Andelman, H. Orland, Phys. Rev. Lett. 79 (1997) 435.
[24] Y. Burak, D. Andelman, Phy. Rev. E 62 (2000) 5296.
[25] S.T. Cui, H.D. Cochran, J. Chem. Phys. 117 (2002) 5850.
[26] H. Berendsen, J. Grigera, T. Straatsma, J. Phys. Chem. 91 (1987) 6269.
[27] E. Lindahl, B. Hess, D. van der Spoel, J. Mol. Mod. 7 (2001) 306.
[28] S. Koneshan, J.C. Rasaiah, R.M. Lynden-Bell, S.H. Lee, J. Phys. Chem. B 102 (1998) 4193.
[29] S. Nose, Mol. Phys. 52 (1984) 255.
[30] J.L. Barrat, L. Bocquet, Phys. Rev. Lett. 82 (1999) 4671.
[31] I. Yeh, M. Berkowitz, J. Chem. Phys. 111 (1999) 3155.
[32] J. Israelachvili, Intermolecular and Surface Forces, Academic Press, New York, 1992.
[33] A.P. Lyubartsev, A. Laaksonen, J. Phys. Chem. 100 (1996) 16410.
[34] C.Y. Lee, J.A. McCammon, P.J. Rossky, J. Chem. Phys. 80 (1984) 4448.
[35] J.P. Valleau, A.A. Gardner, J. Chem. Phys. 86 (1987) 4162.
[36] G.N. Patey, G.M. Torrie, Chem. Scripta 29A (1989) 39.
[37] S.H. Lee, P.J. Rossky, J. Chem. Phys. 100 (1994) 3334.
[38] S.B. Zhu, G.W. Robinson, J. Chem. Phys. 94 (1991) 1403.
[39] I. Benjamin, J. Chem. Phys. 97 (1992) 1432.
[40] F.W. Starr, J.K. Nielsen, H.E. Stanley, Phys. Rev. E 62 (2000) 579.
[41] R.C. Weast, CRC Handbook of Chemistry and Physics, 66th ed., CRC Press, Cleveland, 1985.